100-W 430-ps all-fiber picosecond laser by using 10-/130-μm ytterbium-doped double-clad fiber and its application in SCS

Junjie Chi · Pingxue Li · Boxing Liang · Yifei Yao · Haowei Hu · Guangju Zhang · Mengmeng Zhang · Chunmei Ma

Abstract We report on a theoretical and experimental study on 100-W picosecond pulsed laser produced in 10-μm-core double-clad fiber. Firstly, we make a theoretical simulation based on four-level rate equation and nonlinear Schrödinger equation. In the theoretical simulation, we prove that 100-W picosecond laser can be produced in 10-μm-core doped fiber and find that the length of the doped fiber has a great impact on the spectrum characteristics of the output laser pulse. Then, based on the theoretical analysis results, we make an experimental study introducing Master Oscillator Power Amplifier technology. We do four sets of comparative experiments using different lengths of the doped fiber: 6, 6.5, 7 and 8 m. As a result, 100 W of average output power is obtained in 10-μm fiber core with 6.5 m length. Its repetition rate is 22.7 MHz, its central wavelength is 1,040 nm, and its pulse width is about 430 ps. Moreover, we use the picosecond laser source to pump the nonlinear photonic crystal fiber (PCF) to produce super-continuum source. With two different kinds of PCF, 30 and 36 W average output power are obtained corresponding to spectral broadening range from 550 to 1,650 nm and from 500 to 1,650 nm, respectively.

1 Introduction

High-average-output-power ultra-short pulse fiber laser, because of their high brightness, good beam quality and convenient thermal management, has a wide range of

J. Chi · P. Li (✉) · B. Liang · Y. Yao · H. Hu · G. Zhang · M. Zhang · C. Ma
Institute of Laser Engineering, Beijing University of Technology, Beijing 100124, China
e-mail: pxli@bjut.edu.cn

applications including industrial manufacture, medical treatment, telecommunications and so on [1–3]. With the development of fiber technology, hundred-watt-scale-average-output-power ultra-short pulse fiber laser has been developed greatly by introducing Master Oscillator Power Amplifier (MOPA) technology. Chen et al. [4] demonstrated an all-fiber picosecond laser with 96 W average power in MOPA configuration in 30-μm fiber core. Chen et al. [5] reported a picosecond fiber MOPA source delivering average output power of up to 100 W by using a 25-μm-fiber-core ytterbium-doped fiber in the master amplifier stage. Wu et al. [6] reported an all-fiber MOPA picosecond fiber laser with an average power of 102 W, and they used a 20-μm-fiber-core doped fiber in the master amplifier. Chen et al. [7] demonstrated an all-fiber picosecond MOPA source with 125 W high-power output in a 15-μm-fiber-core doped fiber. Dupriez et al. [8] demonstrated a 321-W-average-power picosecond pulse source in a 43-μm-fiber-core doped fiber. Chen et al. [9] reported a 1.06-μm ytterbium-doped fiber MOPA source delivering average power of 100 W using a 20-μm-fiber-core doped fiber. Moreover, super-large mode area rod-type photonic crystal fiber (PCF) has been used in ultra-short pulsed fiber laser system to obtain a kilowatt-scale high-average-power laser output [10–12].

To sum up, we could find that there are many good results in picosecond fiber laser with the average output power up to 100 W, but for reducing the nonlinear effect, they usually introduce a large fiber-core doped fiber (≥15 μm) or even a rod-type PCF in their power amplifier. Large fiber core diameter provides advantages in terms of higher pump absorption, lower nonlinear effects and higher damage threshold. At the same time, it also means that multimode can be supported in the fiber laser system. In addition, the expensive and complex fiber processing

technology, such as the large-diameter fiber cleaving and large-diameter fiber splicing, are necessary to perform the large core fiber [13, 14]. Rod-type PCF fiber amplifiers mostly introduce spatial light structure, and it does not achieve all-fiber structure. It is mainly due to that the PCF holes collapse will cause large splicing loss or even splicing failure in the fiber splicing process. As we know, in many applications, the fiber amplifier output with good beam quality is necessary for the high-power output. Moreover, in the generation of SCS, picosecond pulsed laser delivered in a small fiber core has important application in pumping the high nonlinear PCF which usually has small fiber core (2–6 μm) in order to yield high nonlinear effects. Therefore, it is very difficult to splice directly the pigtail fiber of the high-power picosecond laser source, which usually has a large core, with the nonlinear PCF in a super-low loss. So it is very valuable to investigate this kind of ultra-short pulse laser produced and delivered in super-small-core fiber with higher output power.

As we know, super-continuum has very important application in many fields, such as Coherent anti-Stokes Raman scattering microscopy [15], stroboscopic white-light interferometry [16], multi-wavelength pulse source [17], frequency metrology [18] and spectroscopy [19]. With the development of PCF technology, using the pulse laser to pump the nonlinear PCF has become a simple and practical way to generate the super-continuum. However, the core diameter of the nonlinear PCF is usually very small (about 2–6 μm), so how to make the pulse pump laser inject the PCF efficiently is a vital problem. There are always two ways to be used: the first is space-coupling injection, which is relatively simple, but also brings many unstable factors for the generated super-continuum [20, 21]. The other is low-loss splicing technology, which needs to use the controlled air-hole collapse technique to expand the core diameter of the PCF and then splicing directly with the pulse fiber laser pump source [22, 23]. This method can greatly improve the coupling efficiency, but this PCF processing technology is very complex. So we make a study on high-power picosecond fiber laser produced in 10-μm fiber core. The aim was to reduce the output-end fiber core size of the pump pulse laser thus to reduce the splicing loss with the small-core nonlinear PCF and increase the coupling efficiency. Moreover, for this 10-μm-fiber-core picosecond laser source, a simple cleaving and splicing technology, which is very suitable for industrial production and application, is only needed.

In this paper, we make a theoretical and experimental study on 100-W-scale-average-output-power picosecond all-fiber pulse laser produced in 10-μm fiber core. Firstly, we established a theoretical model in the Fiberdesk software based on four-level rate equation (FLRE) and nonlinear Schrödinger equation (NLSE). Secondly, according to the theoretical analysis, we make an experimental study for 100-W-scale-average-output-power picosecond all-fiber pulse laser produced in 10-μm fiber core. At last, we obtain a 100-W-average-output-power pulse laser. Its central wavelength is 1,040 nm, repetition rate is 22.7 MHz, pulse width is 430 ps, and signal pulse energy is 4.41 μJ. Furthermore, we use the picosecond laser source to pump the nonlinear PCF to produce super-continuum source. With two different kinds of PCF, 30 and 36 W average output power are obtained corresponding to spectral broadening range from 550 to 1,650 nm and from 500 to 1,650 nm, respectively.

2 Theory analysis

We established a theoretical model in the Fiberdesk software. The approximated system used in Fiberdesk leads to the Eqs. 1–4 for the forward- and backward-propagating signal and pump powers including amplified spontaneous emission (ASE) (www.fiberdesk.com):

$$\frac{dP_P^+}{dz} = \left(\sigma_p^e n_2 - \sigma_p^a n_1 + \alpha_p\right)\Gamma_p \cdot P_P^+ \cdot \sigma_p^e - \sigma_p^e n_2 \cdot 2 \cdot h\nu_p \cdot \Delta\upsilon$$

(1)

$$\frac{dP_P^-}{dz} = -\left(\sigma_p^e n_2 + \sigma_p^a n_1 + \alpha_p\right)\Gamma_p \cdot P_P^+ \cdot \sigma_p^e + \sigma_p^e n_2 \cdot 2 \cdot h\nu_p \cdot \Delta\upsilon$$

(2)

$$\frac{dP_s^+}{dz} = \left(\sigma_s^e n_2 - \sigma_s^a n_1 + \alpha_s\right)\Gamma_s \cdot P_s^+ \cdot \sigma_s^e - \sigma_s^e n_2 \cdot 2 \cdot h\nu_s \cdot \Delta\upsilon$$

(3)

$$\frac{dP_s^-}{dz} = -\left(\sigma_s^e n_2 + \sigma_s^a n_1 + \alpha_s\right)\Gamma_s \cdot P_s^+ \cdot \sigma_s^e + \sigma_s^e n_2 \cdot 2 \cdot h\nu_s \cdot \Delta\upsilon$$

(4)

where z is the axial position of the fiber, $P_{p/s}^\pm$ is the forward or reverse pump power and signal power at z position of the fiber, $\sigma_{p/s}^e$ and $\sigma_{p/s}^a$ are the emission cross section and absorption cross section of the pump or signal light, $\Gamma_{p/s}$ is the fill factor of the pump or signal light, n_2 and n_1 are the upper and lower level particle number of stimulated emission four-level system, $\alpha_{p/s}$ is the additional loss for the fields, $\nu_{p/s}$ is the light frequency of the pump or signal, $\Delta\upsilon$ is the gain bandwidth. For the ultra-short pulse propagation, the rate equations are combined with the NLSE as follows (5):

$$\frac{\partial A}{\partial z} + \frac{\alpha - g}{2}A + \frac{i\beta_2}{2}\frac{\partial^2 A}{\partial T^2} = i\gamma|A|^2 A$$

(5)

where A is the normalized pulse amplitude, β_2 is the second-order dispersion coefficient, γ is the nonlinear coefficient, and α and g are additional loss and gain in fiber.

The approximated system setup diagram is shown in Fig. 1, which includes four parts: signal input, pump input, ytterbium-doped fiber and output part. The parameters in theory analysis are given in Table 1 in detail. In the Fiberdesk software, we set the parameters of the software as follows: the value of β_2 (second-order dispersion) at 1,040 nm is 0.025 ps^2/m, the value of E_g (gain saturation energy) is
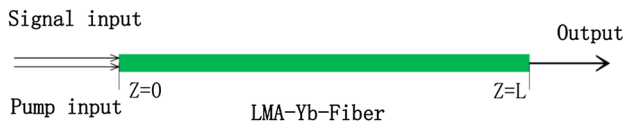
8 μJ, and the value of γ (nonlinear coefficient) is 0.0024 (W m)$^{-1}$.

Firstly, we make a study on relationship between the doped fiber length and the output power. Through theory simulation analysis, we obtain data as shown in Fig. 2. From the simulation data curve, we can find that the 10-μm-core fiber could be used to produce picosecond pulse laser with the average output power up to 100 W. When the doped fiber length is ~6.5 m, the output power is the maximum. When the doped fiber length is greater than ~7 m, the output power begins to reduce due to the strong nonlinear effect.

Then, keeping other parameters unchanged, we make a simulation analysis with different doped fiber lengths: 6,

Fig. 1 Approximated theory simulation diagram

Table 1 Data sheet of the theory simulation

Signal input part	Pump input part	Doped fiber part
Input power: 3 W	Max pump power: 140 W	Fiber type: 10/130 μm (core/cladding)
Central wavelength: 1,040 nm	Pump wavelength: 976 nm	976 Absorption coefficient: 3.9 dB/m
Repetition rate: 22.7 MHz		Fiber length: 6 m/6.5 m/7 m/8 m
Pulse width: 500 ps		

Fig. 2 Theoretical output power versus the length of the ytterbium-doped fiber
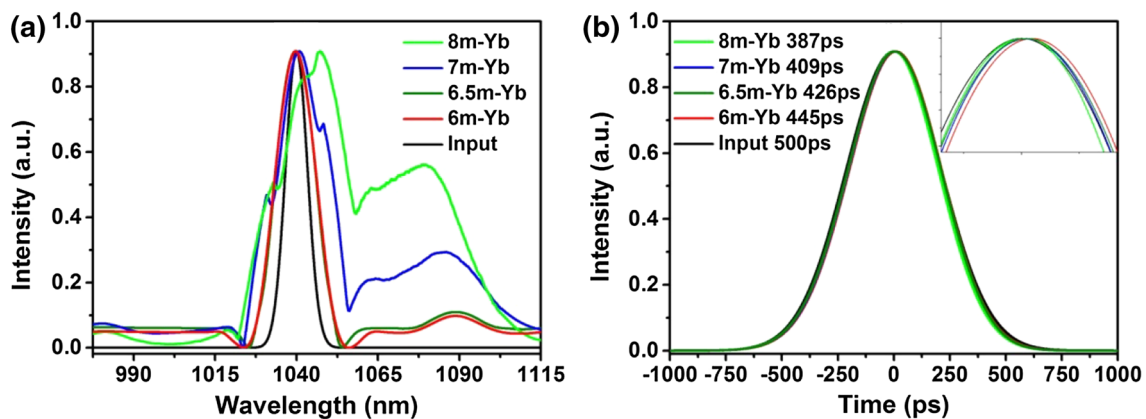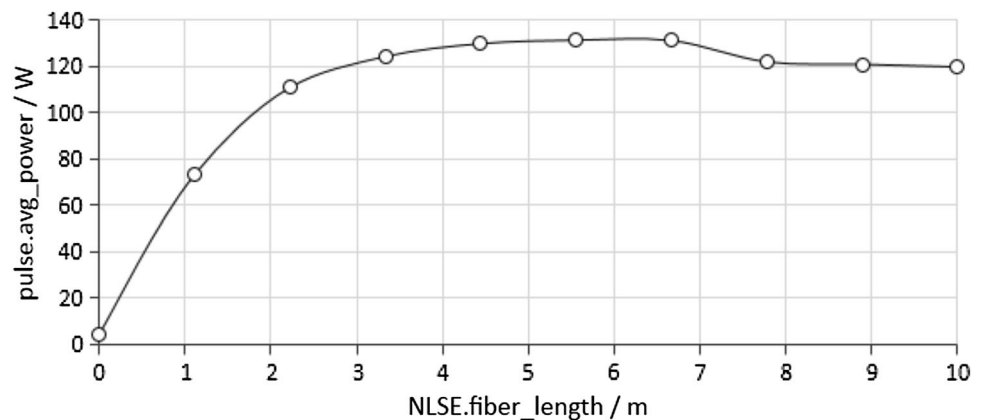

Fig. 3 **a** The theoretical optical spectra of the amplified laser with different lengths of ytterbium-doped fiber. **b** The theoretical pulse width of the amplified laser with different lengths of doped fiber, the *inset* is the partial enlarged view

6.5, 7, and 8 m. As shown in Fig. 3, for frequency domain, we find that the spectrum width will be broadening at 1,090 nm, which is mainly due to the self-phase modulation (SPM), when the doped fiber length becomes longer. There is a little spectral shift toward the long wavelength, when the doped fiber length becomes longer. Moreover, for time domain, we can find that pulse shapes are basically consistent with the different lengths of ytterbium-doped fiber. The pulse width becomes small with the doped fiber length increasing.

## 3 All-fiber MOPA laser system experiments and results

The whole experimental configuration is a typical all-fiber MOPA amplifier, which consists of a passively mode-locked picosecond pulse fiber oscillator as a seed source and a two-stage ytterbium-doped all-fiber amplifier, as shown in Fig. 4. The seed source's average output power is 70 mW with repetition rate of 22.7 MHz, and its pulse width is ~500 ps. Then, after a fiber isolator is used to prevent the preamplifier's backward reflection to the seed source, the seed laser is injected into the preamplifier. The first stage is a ~4-m-long cladding pumped fiber amplifier using ytterbium-doped fiber (10-μm core, NA = 0.075; 130-μm inner cladding, NA = 0.46, ~4.8 dB/m absorption) and is pumped by a 25-W, 976-nm pump coupled into the inner cladding using a fiber combiner. The combiner's pump input part and signal input/output parts are 105-/125-μm core/cladding diameter fiber and 10-/130-μm core/cladding diameter fiber, respectively. Then, through a high-power fiber isolator, the signal is injected into the final high-power fiber master amplifier stage which consisted of the same ytterbium-doped fiber with 10-μm fiber core, six 976-nm LDs and a (6 + 1) × 1 fiber combiner. The combiner's pump part and signal input/output parts are 105-/125-μm core/cladding diameter fiber and 10-/130-μm core/cladding diameter fiber, respectively. Finally, a non-doped fiber mode-expanding end-cap made in our laboratory is spliced to the output end of the MOPA.

Based on the theoretical analysis, we make four sets of experiments by changing the doped fiber length. Firstly, we introduce an 8-m doped fiber into the master amplifier. As shown in Fig. 5a, when the pump power is about 60 W, the average output power is about 40 W. If we continue to increase the pump power, the output power can hardly increase. From the spectrum image shown in Fig. 5b, we can find that when the output power is about 47 W, the

spectra has been broadened to 1,100 nm. And the spectral amplitude from 1,070 to 1,100 nm will be increased, while the pump power is increased, which means there is a very strong nonlinear effect in the doped fiber. Too long fiber will produce ASE, and there is a bump in the 1,090 nm, where it is just a position of Raman frequency shift characteristic spectrum corresponding to the 1,040-nm laser. So there may be two kinds of nonlinear effects: SPM and Stimulated Raman Scattering (SRS). This is why the output power is hardly increased, which may be due to the strong SPM. Finally, when the pump power is 125 W, a output power of 51 W is obtained. Secondly, we make the doped fiber shortened to 7 m. From the spectrum image shown in Fig. 5c, we can find that when the output power is about 57 W, there will be a little bump and spectral broadening in 1,090 nm, which is same as the one of 8-m doped fiber experiment. And when the pump power is continuously increased, the phenomenon of the bump and spectral broadening in 1,090 nm will become more serious. Although the nonlinear effects of SPM and SRS decrease a lot, it still exists here. So it still has a certain effect on the output power of the amplifier. This is the main reason to limit the output power of the amplifier, as shown in Fig. 5a. Finally, when the pump power is 125 W, the 76 W output power is obtained. Thirdly, we continue to shorten the doped fiber to 6.5 m. When the pump power is 140 W, the 100 W average output power is generated in the amplifier. The optical-to-optical conversion efficiency is about 71.4 %. From the spectrum image shown in Fig. 5d, there is only a small bump in 1,090 nm, when the output power is 100 W. Moreover, the input–output curve is approximately linear shown in Fig. 5a. At last, we introduce the 6-m doped fiber in the master amplifier. When the pump power is 140 W, the average output power is about 95 W. In Fig. 5a, we can find the input–output curve of the 6-m doped fiber amplifier is also approximately linear, but its slope efficiency is lower than the result of the 6.5-m doped fiber amplifier. This may be because of that the 6-m doped fiber cannot provide enough gain for the amplifier system, although the nonlinear effect is almost entirely suppressed. From the spectrum image shown in Fig. 5e, the spectral curve is relatively similar with the one of the 6.5-m doped fiber amplifier. The spectral characteristics of the experimental data are very consistent with our theory analysis, which suggests that the 6.5-m-long doped fiber is the optimal length to produce 100-W picosecond pulse laser in 10-μm fiber core.

The output laser of the 6.5-m doped fiber amplifier is detected by a high-speed digital oscilloscope (LyCroy

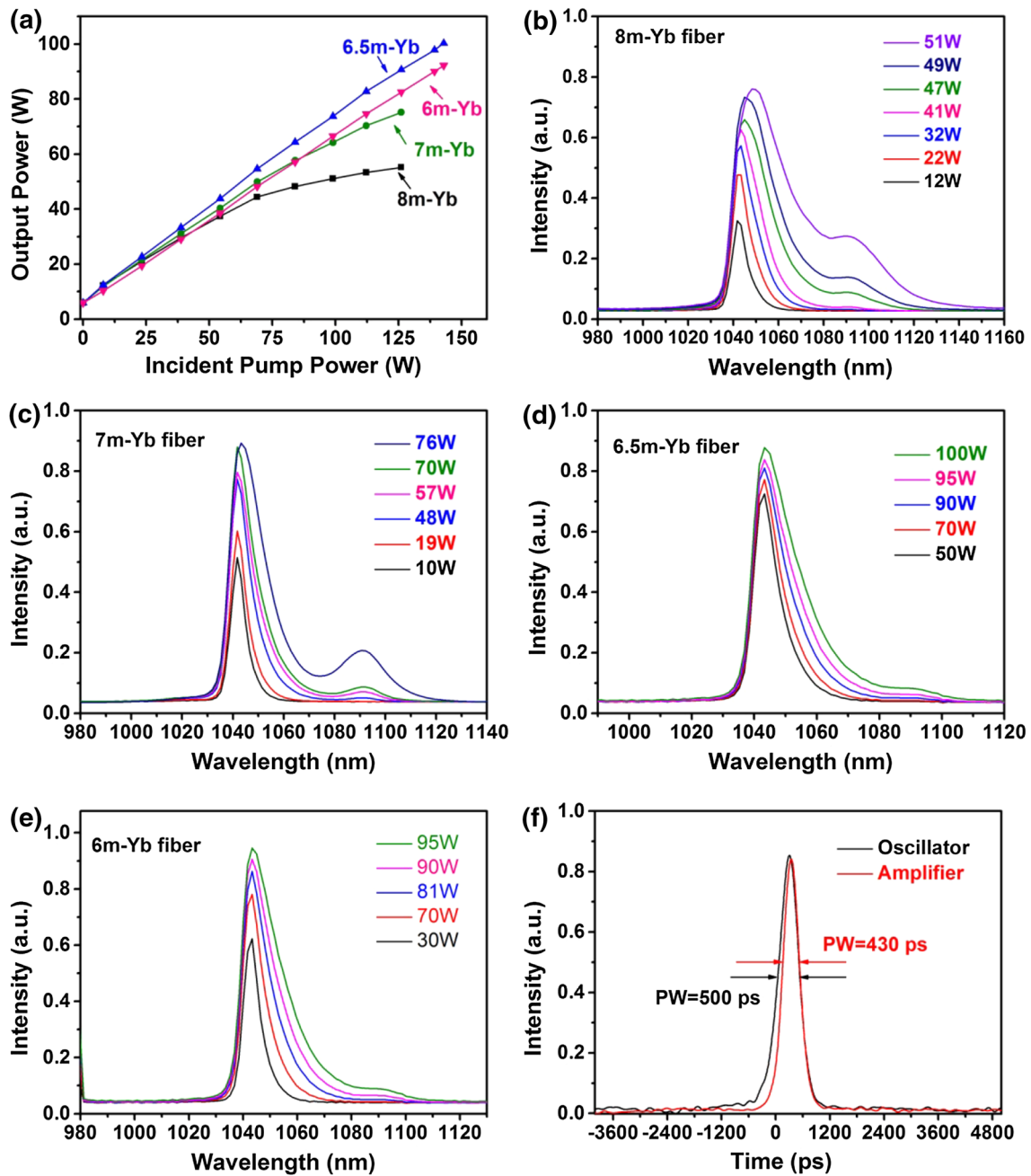**Fig. 4** Experimental configuration of the 100-W pulse laser
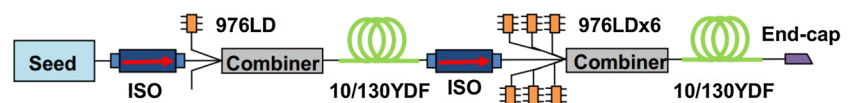
Fig. 5 **a** The input–output curves of the MOPA system with different lengths of doped fiber, **b** the spectra *curve* of the 8-m doped fiber MOPA system, **c** the spectra *curve* of the 7-m doped fiber MOPA system, **d** the spectra *curve* of the 6.5-m doped fiber MOPA system, **e** the spectra *curve* of the 6-m doped fiber MOPA system, **f** the pulse width *curves* of the oscillator and the 6.5-m doped fiber MOPA system

20 GHz), and its pulse width is about 430 ps. In Fig. 5f, we can find the pulse width (430 ps) of the amplified laser becomes small relative to the signal light (500 ps). Normally, pulse width of amplified laser should be larger than the signal laser, which is caused by positive dispersion of the amplifier system. This opposite phenomenon may be caused by another mechanism, that is, gain saturation [24–26]. Because of the gain effect's time dependence, gain saturation for pulse frontier edge is weaker than pulse trailing edge, which will result in pulse narrowing in time domain. The time-domain characteristics of the experimental data also show the validity of our theoretical analysis. Figure 6 is the pulse trains of the MOPA system output laser, which is stable and uniform.

4 SCS experiments and results

We also make a study on SCS using the picosecond pulse laser obtained above to pump the nonlinear PCF. The experimental configuration is shown in Fig. 7. It concludes three parts: the picosecond pulse laser source, the transition fiber and the PCF. The picosecond pulse laser source is obtained by MOPA technology, as mentioned above. Its average output power is 100 W with the repetition rate of 22.7 MHz and its pulse width is 430 ps. The transition fiber is 6-/125-μm core/cladding fiber, which is used to reduce the mode field mismatch between the laser source and the PCF. One end of it is spliced with the 10-/130-μm output
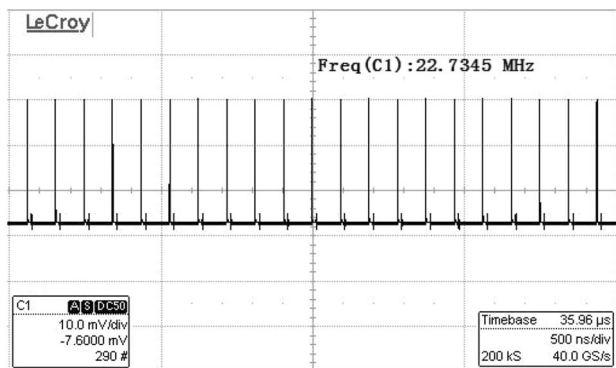

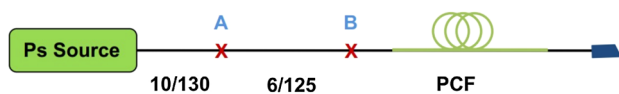**Fig. 6** Pulse trains of the amplified laser

Fig. 7 Setup of the super-continuum source system

end of the picosecond laser source, as shown at "A" point in Fig. 7. The other end of the transition fiber is spliced with the PCF directly using a low-loss splicing program, as shown at "B" point in Fig. 7. At last, an 8° angle cap made by us is spliced to the output end of the whole system, which is used to avoid laser feedback.

In the experiment, we introduce two kinds of PCF to make a SCS research. The cross-sectional view of the first PCF is shown in Fig. 8a. Its structure consists of a sold silica core, surrounded by 5 rings of round-arrangement air holes to ensure sufficiently low confinement loss. The pitch, which is the distance between two most adjacent holes, is 3.9 ± 0.1 μm, the zero dispersion wavelength is $1,030 \pm 20$ nm, the mode field diameter is 4.5 ± 0.1 μm, and the nonlinear coefficient at 1,060 nm is 11 (W km)$^{-1}$. The cross-sectional view of the second PCF is shown in Fig. 8b. Its structure consists of a sold silica core, surrounded by 5 rings of hexagonal-arrangement air holes to ensure sufficiently low confinement loss. The pitch, which is the distance between two most adjacent holes, is 5.9 ± 0.1 μm, the zero dispersion wavelength is $1,040 \pm 20$ nm, the mode field diameter is 6.4 ± 0.1 μm, and the nonlinear coefficient at 1,060 nm is 9 (W km)$^{-1}$.

Firstly, we introduce the round-arrangement air-hole PCF into our super-continuum experiment and its length is about 7.5 m. When the picosecond laser source is 76 W, 30 W output power of the super-continuum source is obtained with spectral broadening range from 550 to 1,650 nm. If we continue to increase the injection power of the laser source, the splicing point in the transition fiber will be burned out. Secondly, the hexagonal-arrangement air-hole PCF is used in our super-continuum experiment and its length is about 6 m. When the picosecond laser source is 85 W, 36 W output power of the super-continuum
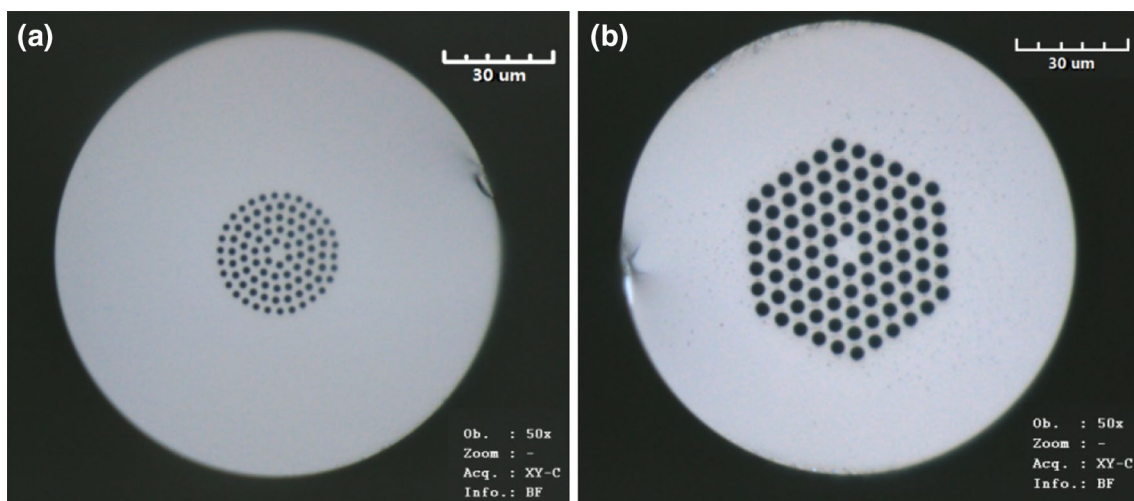

Fig. 8 a Cross-sectional view of the round-arrangement air-hole PCF, **b** cross-sectional view of the hexagonal-arrangement air-hole PCF
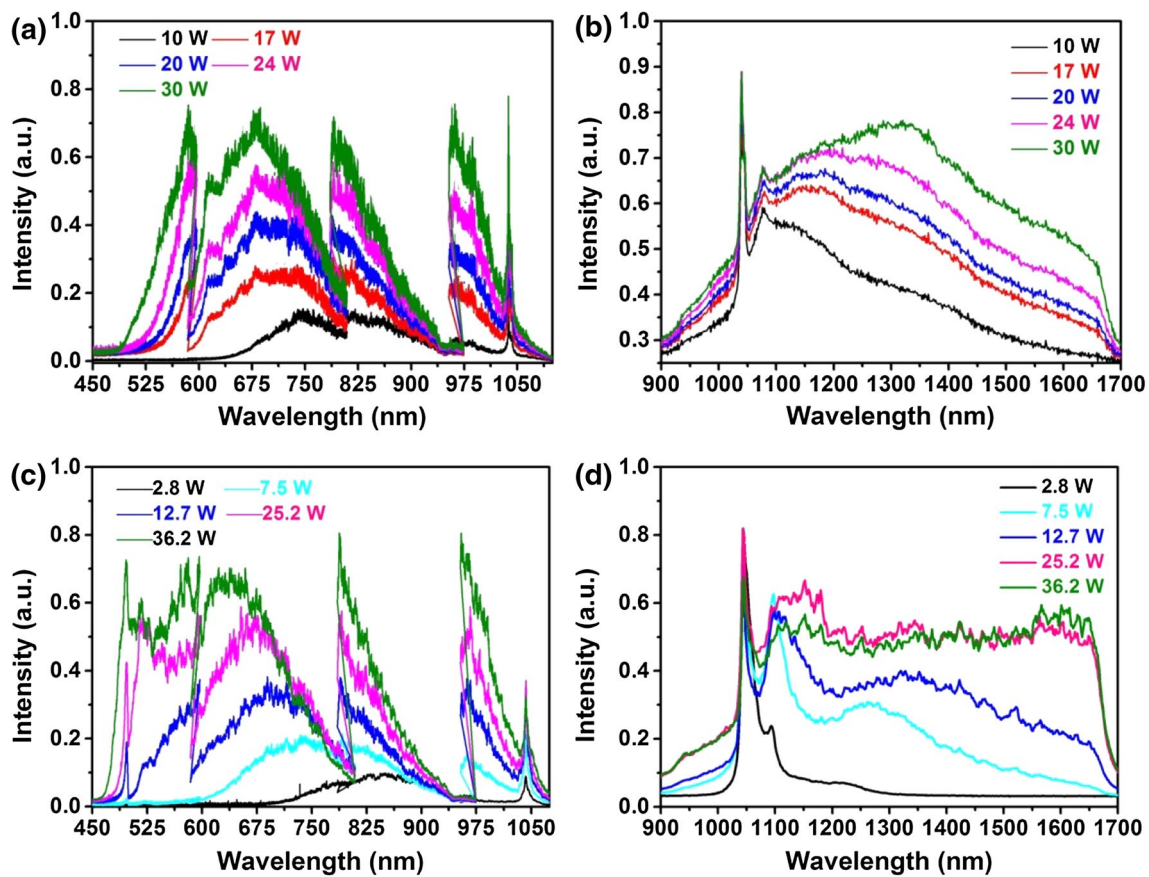
Fig. 9 a Short-wavelength optical spectrum produced in the round-arrangement air-hole PCF, **b** long-wavelength optical spectrum produced in the round-arrangement air-hole PCF, **c** short-wavelength optical spectrum produced in the hexagonal-arrangement air-hole PCF, **d** long-wavelength optical spectrum produced in the hexagonal-arrangement air-hole PCF

source is generated with spectral broadening range from 500 to 1,650 nm. In order to protect the devices, we do not further increase the injection laser power. The super-continuum spectra generated from the PCF are observed by two optical spectrum analyzers with measurement ranges from 350 to 1,075 nm (AvaSpec-NIR256, resolution: 0.05 nm) and from 900 to 1,700 nm (Ocean Optics Spectrometer-NIRQ512, resolution: 3 nm). Fig. 9a, b shows the process of spectral broadening with the average power of the super-continuum from 10 to 30 W, which is produced in the round-arrangement air-hole PCF. And Fig. 9c, d shows the process of spectral broadening with the average power of the super-continuum from 2.8 to 36 W, which is produced in the hexagonal-arrangement air-hole PCF. Our AvaSpec is a high-precision spectrometer, and it is composed of four channels: 339–596, 583–809, 785–974 and 953–1,100 nm. So short-wave spectra measured by it are not very smooth, as shown in Fig. 9a, c.

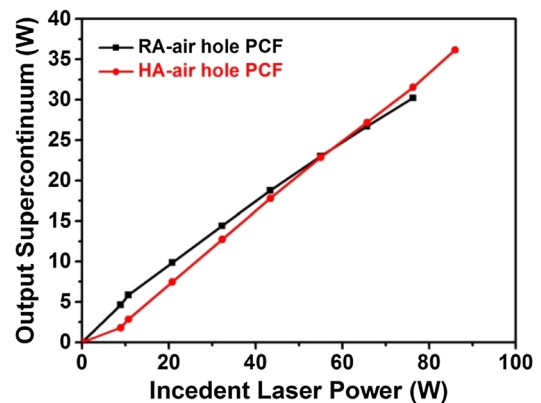The input–output curve data of the two different PCF are shown in Fig. 10, and the average output power of the super-continuum source increases almost linearly with the incident laser power. Moreover, the pulse width of the output super-continuum laser is detected by a high-speed digital oscilloscope (LyCroy 20 GHz). Figure 11 shows the super-continuum laser pulse trains that are very stable and
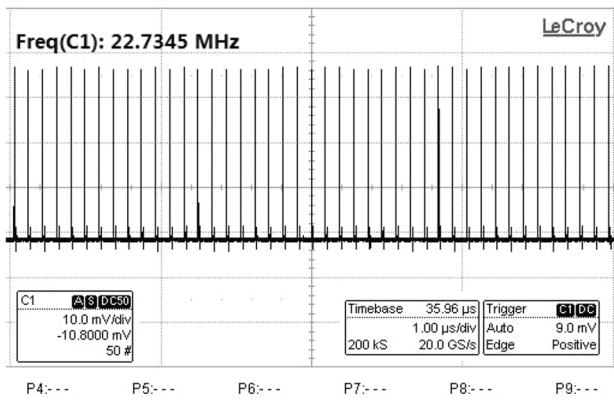

Fig. 10 Input–output curves of the super-continuum system with different PCF, *RA* round arrangement, *HA* hexagonal arrangement

Fig. 11 Super-continuum laser pulse trains detected by LyCroy high-speed oscilloscope
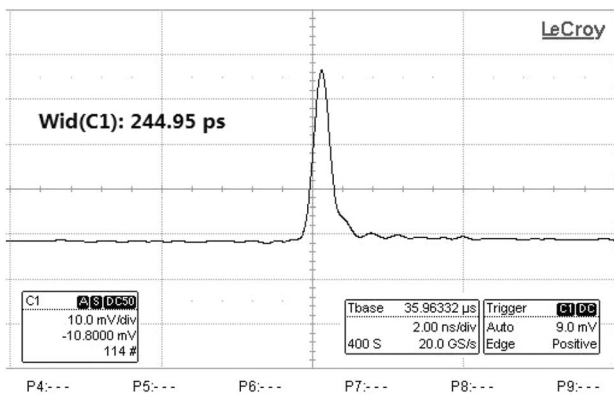

Fig. 12 Pulse width of the super-continuum laser pulse detected by LyCroy high-speed oscilloscope

uniform just like the pump laser from pump laser source, which implies that there is good time coherence for the super-continuum laser [27–29]. Figure 12 shows the pulse width of the super-continuum laser, which is about 244.95 ps. Its pulse width is also narrowed relative to the pump laser source, which is about 430 ps.

5 Conclusion

We demonstrate a 100-W-average-output-power picosecond pulse laser produced in 10-μm fiber core not only from theory simulation, but also from experiment. Firstly, we established a theoretical model in the Fiberdesk software based on four-level rate equation (FLRE) and nonlinear Schrödinger equation (NLSE). Secondly, according to the theoretical analysis, we make an experimental study for 100-W-scale-average-output-power picosecond all-fiber pulse laser produced in 10-μm fiber core. Through changing doped fiber length with 8, 7, 6.5 and 6 m, we find the

pulse shape of the frequency domain is relatively good in 6.5-m doped fiber MOPA system and its average output power characteristics are relatively better. At last, we obtain a 100-W-average-output-power pulse laser in 6.5-m-long 10-μm fiber core. Its central wavelength is 1,040 nm, repetition rate is 22.7 MHz, pulse width is 430 ps, and signal pulse energy is 4.41 μJ. Furthermore, we use the picosecond laser source to pump the nonlinear photonic crystal fiber (PCF) to produce super-continuum source. With two different kinds of PCF, one is round-arrangement air holes structure and the other is hexagonal-arrangement air holes structure. Finally, 30 and 36 W average output powers are obtained corresponding to spectral broadening range from 550 to 1,650 nm and from 500 to 1,650 nm, respectively. The pulse width of the super-continuum laser is about 244.95 ps, the pulse trains of it are very uniform and it shows good time coherence in broadening wave band.

References

1. H. Pan, D. Lee, S.H. Ko, C.P. Grigoropoulos, H.K. Park, T. Hoult, Appl. Phys. A **104**, 29 (2011)
2. N.M. Fried, Laser Surg. Med. **36**, 52 (2005)
3. A. Martinez, S. Yamashita, Opt. Express **19**, 6155 (2011)
4. S.P. Chen, H.W. Chen, J. Hou, Z.J. Liu, Opt. Express **17**, 24008 (2009)
5. K.K. Chen, S. Alam, D. Lin, A. Malinowski, D.J. Richardson, in *Conference on Lasers and Electro-Optics/International Quantum Electronics Conference, Optical Society of America*, paper CWK2 (2009)
6. W.D. Wu, T.Q. Ren, J. Zhou, S.T. Du, X.J. Gu, Q.H. Lou, Chin. Phys. Lett. **28**, 114206 (2011)
7. H.W. Chen, Y. Lei, S.P. Chen, J. Hou, Appl. Phys. B **109**, 233 (2012)
8. P. Dupriez, A. Piper, A. Malinowski, J.K. Sahu, M. Ibsen, Y. Jeong, L.M.B. Hickey, M.N. Zervas, J. Nilsson, D.J. Richardson, in *Optical Fiber Communication Conference, Optical Society of America*, paper PDP3 (2005)
9. K.K. Chen, J.H.V. Price, S. Alam, J.R. Hayes, D. Lin, A. Malinowski, D.J. Richardson, Opt. Express **18**, 14385 (2010)
10. P. Wan, L.M. Yang, J. Liu, Opt. Express **21**, 29854 (2013)
11. T. Eidam, S. Hanf, E. Seise, T.V. Andersen, T. Gabler, C. Wirth, T. Schreiber, J. Limpert, A. Tünneermann, Opt. Lett. **35**, 94 (2010)
12. Z. Zhao, B.M. Dunham, F.W. Wise, J. Opt. Soc. Am. B **31**, 33 (2014)
13. P.X. Li, Z.Q. Zhao, J.J. Chi, C. Yang, G.J. Zhang, H.W. Hu, Y.F. Yao, Y. Li, X.F. Wang, G.S. Zhong, Opt. Commun. **317**, 62 (2014)
14. J. Limpert, S. Hoffer, A. Liem, H. Zellmer, A. Tunnermann, S. Knoke, H. Voelckel, Appl. Phys. B **75**, 477 (2002)
15. P. Klarskov, A. Isomäki, K.P. Hansen, P.E. Andersen, Opt. Express **19**, 26672 (2011)
16. S. Novotny, V. Durairaj, I. Shavrin, L. Lipiäinen, K. Kokkonen, M. Kaivola, H. Ludvigsen, Opt. Express **22**, 13625 (2014)
17. T. Mori, T. Yamamoto, K. Kurokawa, S. Tomita, IEICE Electron. Expr. **7**, 1504 (2010)

18. R. Holzwarth, Yh Udem, T.W. Hänsch, J.C. Knight, W.J. Wadsworth, P.St.J. Russell, Phys. Rev. Lett. **85**, 2264 (2000)
19. K. Lindfors, T. Kalkbrenner, P. Stoller, V. Sandoghdar, Phys. Rev. Lett. **93**, 037401 (2004)
20. R. Cherif, M. Zghal, I. Nikolov, M. Danailov, Opt. Commun. **283**, 4378 (2010)
21. J.L.H. Kho, C.A. Rohde, F. Vanholsbeeck, M.C. Simpson, Opt. Commun. **294**, 250 (2013)
22. H.W. Chen, Z.L. Chen, S.P. Chen, J. Hou, Q.S. Lu, Appl. Phys. Express **6**, 032702 (2013)
23. H.W. Chen, S.P. Chen, J.H. Wang, Z.L. Chen, J. Hou, Opt. Commun. **284**, 5484 (2011)
24. A. Malinowski, K.T. Vu, K.K. Chen, J. Nilsson, Y. Jeong, S. Alam, D.J. Lin, D.J. Richardson, Opt. Express **17**, 20927 (2009)
25. D.N. Schimpf, C. Ruchert, D. Nodop, J. Limpert, A. Tunnermann, F. Salin, Opt. Express **16**, 17637 (2008)
26. G. Sobon, P. Kaczmarek, A. Antonczak, J. Sotor, A. Waz, K.M. Abramski, Appl. Phys. B **105**, 721 (2011)
27. K.R. Khan, M.F. Mahmood, A. Biswas, IEE J. Sel. Top. Quant. **20**, 7500309 (2014)
28. N. Nishizawa, Opt. Fiber Technol. **18**, 394 (2012)
29. L.E. Hooper, P.J. Mosley, A.C. Muir, W.J. Wadsworth, J.C. Knight, Opt. Express **19**, 4902 (2011)